UNIVERSITY OF CALIFORNIA

Los Angeles

Effect of Structured Channels on Controlling Interparticle Spacing in Inertial Microfluidics

A thesis submitted in partial satisfaction

of the requirements for the degree Master of Science

in Biomedical Engineering

by

Dianne Pulido

2012

ABSTRACT OF THE THESIS

Effect of Structured Channels on Controlling
Interparticle Spacing in Inertial Microfluidics

by

Dianne Pulido

Master of Science in Biomedical Engineering
University of California, Los Angeles, 2012
Professor Dino Di Carlo, Chair

Single-cell microfluidic analysis platforms are powerful tools in the characterization of rare phenotypes that exist as subpopulations and may be hidden by bulk averages. Operating at high throughputs and high concentrations is often necessary for processing large volumes required to isolate these rare populations and obtain statistical relevance. The current challenge of working at high concentrations lies in the inability of systems to perform relevant analysis or separation with high accuracy or purity when the interparticle spacing is reduced beyond the system response time, resulting in coincident events. This work proposes the use of structured channels to control interparticle spacing with an inertial microfluidics platform capable of operating at high throughputs (up to 10,000 particles/sec), high concentrations (1-3 million particles/mL), and with heterogeneous cell populations (16% cell size variation). Local expansion-contraction structures and extended chambers are used in series to induce secondary flows that promote repulsion between neighboring particles reliably (>98%) beyond a 40-μm threshold. This use of

passive methods to control spacing presents a more robust alternative to active methods such as squeezing sheath fluid or electric and magnetic field manipulation.

The thesis of Dianne Pulido is approved.

Daniel T. Kamei

Eric Pei-Yu Chiou

Dino Di Carlo, Committee Chair

University of California, Los Angeles

2012

TABLE OF CONTENTS

LIST OF FIGURES

ACKNOWLEDGEMENTS

I thank my advisor Professor Dino Di Carlo for his support in my work, for sharing his knowledge, and for always having an open door. Similarly, I thank my committee members Daniel T. Kamei and Eric Pei-Yu Chiou for their help and attention. I would also like to thank Aram J. Chung for his valuable insight, patience in teaching, and for answering my numerous questions, as well as Hamed Amini for his aid in numerical simulations and readiness to always discuss. Finally, I thank Matt for hanging in there and always giving me a catch, Beayna for being my lifeline and trusty accomplice, and my parents for encouraging me through the years. This one is for you.

INTRODUCTION

Microfluidic platforms have proven to be powerful approaches in the manipulation and analysis of single cells and particles in flow, such as in separation[1–5], sample preparation[4,6], optical characterization[7,8], and mechanical phenotyping[9–11] of heterogeneous populations. Achieving single-cell analysis is important for characterizing abnormalities or rare phenotypes that exist as subpopulations in a large sample and may otherwise be hidden in bulk averages, such as in the identification of circulating tumor cells (CTCs) or stem cells in blood[12,13]. Since these populations of interest can be rare, microfluidic techniques that can process large samples at high throughputs, while still maintaining the required specificity, provide practical solutions to the challenge of obtaining quantitative measures at statistical levels in a reasonable amount of time. Moreover, high-throughput systems have a robustness that may facilitate their translation out of the research field and into clinical applications where they are needed.

One approach to achieving higher throughputs is to improve the particle sorting or particle analysis component of the microfluidic platform. For example, in the case of fluorescence-activated cell sorting (FACS), improving the response time of the optical components would allow for quicker detection of single cells and more rapid sorting. However, in many such applications, the external optical or electrical components are currently optimized to a high level of efficiency and rapid turnover;[2] the bottleneck to higher throughputs instead remains in the system's ability to operate at high particle concentrations while also preventing coincident detection events.

Operating at higher concentrations minimizes the amount of time between events and in this manner increases throughput, but comes at a cost to purity because of the challenge with ensuring the appropriate spatial frequency for single-cell isolation or separation techniques[14].

In the case of droplet microfluidics, obtaining the correct spatial frequency of particles as they travel downstream to the encapsulation region is key to ensuring that the number of empty droplets is minimized and that few droplets contain more than one cell or particle for analysis[14,15]. Similarly, in flow cytometry, the space between particles as they cross the optical interrogation zone should be great enough so that only one particle or cell is in the laser spot at any time for accurate fluorescence detection.

The control of spatial frequency of particles is therefore important to maintaining throughput and efficiency in single-cell platforms. Methods to address this spacing issue include the use of active elements to force neighboring particles apart, such as squeezing sheath fluids or applied electrical or magnetic fields[16,17]. For example, conventional flow cytometers use co-axial sheath flow in capillaries to both focus and space particles before optical measurements at throughputs of 10-25,000 cells/sec[16]. Although this does provide a solution to spacing control, the use of large amounts of sheath fluid presents an extra resource that must be consumed, adding cost and energy to the system. Furthermore, achieving higher throughputs through this method results in the consumption of greater volumes of sheath fluid, which creates unwanted waste and limits run-time for experiments, as the fluid must be replenished. The use of applied external forces for particle manipulation similarly comes at a cost to the energy and the simplicity of the system.

The passive manipulation of particles in flow, with no additional external forces or sheath fluids, would be an elegant solution to spacing control and a step towards increasing throughput in single-cell microfluidic platforms while maintaining robustness for point-of-care applications. The emerging field of inertial microfluidics has specifically demonstrated recent advancements in passive particle control in microchannels and the possibility of operation at throughputs as high as 1 million cells/sec[12,18]. Furthermore, inertial forces in these platforms have been shown

to scale with velocity, thereby supporting the aim of achieving high throughputs while maintaining system simplicity. Using this toolbox, inertial microfluidics is a viable option for the improvement of single-cell analysis techniques.

1.1 Inertial Microfluidics

Traditional microfluidics operates under the Stokes flow assumption that the inertia of the fluid is negligible, such that the system's Reynolds number (*Re*) can be approximated to be zero, where *Re* is the ratio of inertial forces to viscous forces. In the following equation, ρ is the density of the fluid, U_m the max fluid velocity, D_h is the hydraulic diameter, and μ is the viscosity of the fluid.

$$Re = \frac{\rho U_m D_h}{\mu}$$

Re is typically estimated to be zero because of the small channel dimensions and low fluid velocities[18]. Although this may be an appropriate estimation for some microfluidic systems, such as in "creeping flow," it becomes necessary to include fluid inertia in the full solution to the Navier-Stokes equation at modest fluid velocities for accurate characterization, leading to non-zero *Re* values (*e.g.,* water flowing through a 100 μm channel at 0.01 m/s has a *Re* approaching 1)[18]. The term "inertial microfluidics" therefore refers to microchannels operating in this finite-Reynolds number regime that can still be described by laminar flow ($1 < Re << 2000$).

1.1.1 Particle Migration

Studies in inertial microfluidics have demonstrated interesting effects to particles in flow, such as the formation of particle "equilibrium" positions, or focusing positions. This self-assembly of particles in inertial flow was first reported to occur in cylindrical macroscale pipes by Segré and Silberberg[19] in 1961, and has only more recently been

explored in microscale channels. Particle focusing occurs from a balance of two inertial lift forces that act on the particle: the shear gradient lift force, which acts to move particles down the gradient in shear rate away from the channel center, and the wall effect lift force that prevents particles from touching the walls of the channel due to an asymmetric wake caused by the particle[20] (Fig. 1.1). A random distribution of particles in a channel operating in an inertial regime will therefore experience lateral migration and assemble to focusing positions downstream. The following equations describe the two inertial lift forces that act on particles of diameter a in a channel of height H (where a is approaching the channel dimensions)[21].

$$F_{L\,shear} \propto \frac{\rho U_m^2 a^3}{H}$$

$$F_{L\,wall} \propto \frac{\rho U_m^2 a^6}{H^4}$$

By this relationship, particles of larger diameter will have greater lift forces; similarly, the lift forces scale with the square of velocity, supporting high-throughput applications. Useful design parameters for these types of channels, such as the length and flow rate required for focusing to occur, have been outlined in a recent review of inertial microfluidics by Di Carlo[18].

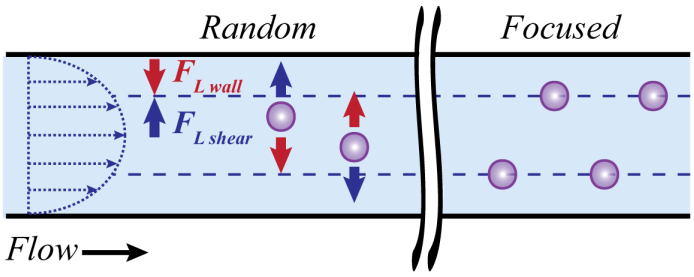

Fig. 1.1: Inertial focusing of particles. *Particles in inertial flow experience two inertial lift forces: the shear gradient lift force ($F_{L\,shear}$) and the wall effect lift force ($F_{L\,wall}$). The shear gradient lift force promotes the migration of particles away from the channel centerline, and the wall effect lift force prevents particles from touching the walls. A balance of these two forces creates particle focusing "equilibrium" positions and results in focused particle streams.*

The phenomenon of inertial focusing is very dependent on the cross-sectional shape of the channel (Fig. 1.2). In the case of Segré and Silberberg, millimeter-sized particles were seen to focus to an annulus in cylindrical pipes. For microfluidic channels with square cross-sections, the number of focusing positions is reduced to four (face-centered on each wall), and for rectangular cross-sections, only two focusing positions exist (face-centered on each of the longer walls)[18]. Taking passive particle manipulation a step further, curving channels have been used to induce secondary flows and promote single-stream ordering in rectangular channels[18,22]. The reduction of focusing positions through passive means (changes to channel geometry alone) has many applications in biological analysis techniques where knowledge of particle positioning is beneficial.

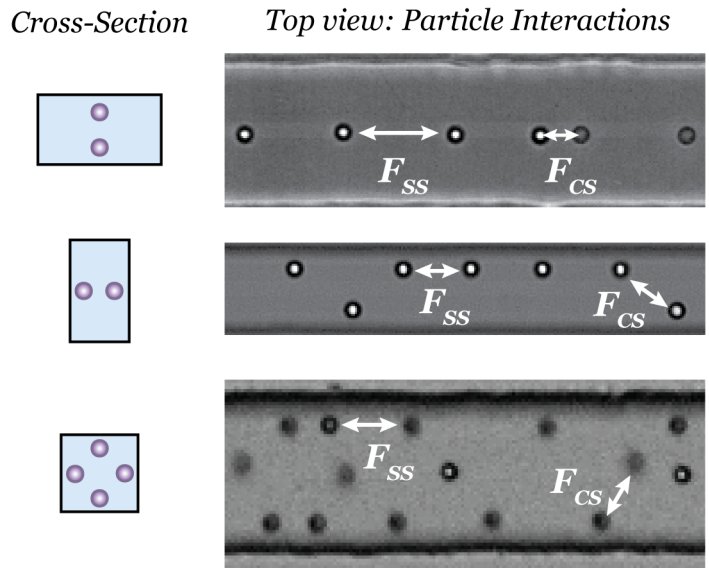

Fig. 1.2: Particle focusing positions and interactions in channels. *The channel cross-section is important in determining the arrangement of particle focusing positions. Particles in the same stream are expected to experience a same-stream force (F_{SS}) and particles across different streams will experience a cross-stream force (F_{CS}).*

1.1.2 Particle Interactions

Particle interactions in inertial microfluidics have been suggested to occur at separation distances less than ~10·a (where a is the particle diameter), and have been shown to consist primarily of repulsive interactions[23]. Particles are observed to self-order in trains at their focusing position and adopt a characteristic spacing through a balance of these interactions, as well as through repulsions caused by the reversing streamlines entrained around particles[24]. The work of Lee *et al.*[23] has also demonstrated how changes to channel geometry through an expansion in channel width have an effect to interparticle spacing, such that particle pairs that traveled through a change in channel width exhibited an increase to their separation distance.

An extension to this approach is to explore the effects of structured channels, or channels with changes to the channel walls and consequently the channel width, to interparticle spacing. Since particles in trains are stabilized to a given separation distance by the reflection of viscous disturbance flows off the channel walls[23], it can be expected that changes to the angle of the wall will have an effect on the ordering of the particles. Furthermore, sudden expansions to the channel width or disturbances to flow have been shown to create interesting fluidic effects, such as the creation of recirculations and secondary flows[25], which suggest that it may be possible to program favorable flows for the manipulation of particle ordering and spacing.

This aim of interparticle spacing manipulation at high particle concentrations would make it unnecessary to dilute the suspensions of interest for single-cell analysis and separation techniques to ensure it is well within the system's measurement capability, thereby minimizing sample preparation time and increasing system throughput.

MATERIALS AND METHODS

2.1 Chip Design and Fabrication

Channels were designed in 2D using AutoCAD, and made into masks for photolithographical etching onto silicon wafers. Microfluidic devices were then made using a standard PDMS (polydimethylsiloxane) replica molding technique. This involved mixing PDMS base and agent (Sylgard 184 Elastomer Kit) in a 10:1 ratio and pouring over the silicon wafer to transfer channel features to the PDMS after curing at 65°C for a minimum of 4 hours. The PDMS was then removed from the wafer and bonded to a glass slide using O_2 plasma activation for 30 seconds. The bonded chips were allowed to bake at 65°C for a minimum of 2 hours before usage.

2.2 Experimental Setup

Flow was driven through the microfluidic chips using a Harvard Apparatus PHD 2000 syringe pump with plastic BD syringes. PEEK tubing (Upchurch Scientific) was used for the inlet and outlet of each channel. Particles tested were prepared from stock solutions (Thermo Scientific) to the desired concentrations with deionized water. For 15- and 19-μm sized particles, a small amount (~0.1-0.3%) of Tween 80 (Fisher Chemical) was added to the suspension to prevent clogging. In the case of cell experiments, MCF7 and Jurkat cells were cultured in tissue culture flasks under common passage procedures. Cells were resuspended in sterile PBS (Fisher, 1x) immediately before testing in microfluidic channels. Images were captured using a Phantom v7.3 high-speed camera (Vision Research, Inc.) with 1-μs exposures.

2.3 Data Analysis

Analysis of images for particle spacing, position, and velocity was done using MATLAB and ImageJ. Fluid flow simulations were done using finite-element analysis with COMSOL 3.4.

SYSTEM FOR SPACING CONTROL

3.1 System Characteristics

A typical inertial microfluidic platform consists of several parameters that affect particle spacing and assembly, such as concentration of the particle suspension and variation in particle size distribution. Engineering a system for the control of interparticle spacing requires an understanding and characterization of these basic parameters, as described below.

3.1.1 Particle Concentration

In inertial microfluidics, particles have been observed self-assemble into lattices and ordered trains at high concentrations[12,20]. As the concentration of a suspension increases, the spacing between particles is reduced and particle-particle interactions become more relevant as particles "feel" the reversing streamlines entrained around their neighbors in inertial flow, similar to the case of confined Stokes flow. These reversing streamlines, in combination with inertial forces that keep particles at focusing positions, have been described as mechanisms for particle ordering and train formation[23,24].

The concentration of the suspension tested is therefore important in designing a microfluidic device that controls interparticle spacing. Concentration can be translated to length fraction (λ) for the case of single-stream focusing of particles for a more relevant measure[18], where λ is related to volume fraction (V_f = *volume of particles/volume of entire solution*) through the following equation: $\lambda = 6WHV_f/\pi a^2$. For example, if a 40 μm minimum spacing is desired between particles with diameter a = 10 μm in a channel of dimensions W = 45 μm and H = 72 μm, the volume fraction

needed to ensure λ = 0.25 would be 0.40%. In reality, any suspension will exhibit a randomness of spacing distributions within a microchannel such that regions of tightly packed particle trains may exist and prevent the system from isolating single particles. An ideal solution to this problem would be the design of a microfluidic channel that can create more uniform spacing, specifically through the expansion of spacing in tight regions to fill neighboring empty regions.

In these experiments, a 40-μm threshold is chosen as a measure for particle expansion and is informed by current flow cytometry and particle sorting response time capabilities[2].

3.1.2 Particle Size

It has been previously reported that there is no significant difference in the velocities of different sized particles[21], despite the fact that the focusing position of larger particles is seen to shift towards the channel centerline and towards faster streamlines. However, data of mixed particle populations acquired in this work indicates that different sized particles travel at different velocities (Fig. 3.1). Specifically, this was seen for the case of mixed 19- and 10-μm particles in a channel with dimensions W = 80 μm and H = 30 μm. The small particles were characterized by a higher velocity (U_1) when found in same-sized particle trains when compared to mixed-sized particle trains (U_2), which have a bimodal distribution in their velocities (Fig. 3.1B). The larger particles were also observed to lead mixed-particle trains, and were characterized in turn by a velocity distribution with a single peak at the slower velocity, U_2. These velocity differences cause fast-traveling particles to approach slower (larger) particles and become entrained behind them, resulting in a contraction to their average interparticle spacing as they slow to adopt the reduced velocity (Fig. 3.1C). Although repulsive interactions between

particles have been shown to dominate ordering and typically result in expansion of spacing, this contraction can be drawn as a parallel to compression on a spring by an applied force, which is expected to return to its relaxed state or "spacing" once the force has dissipated.

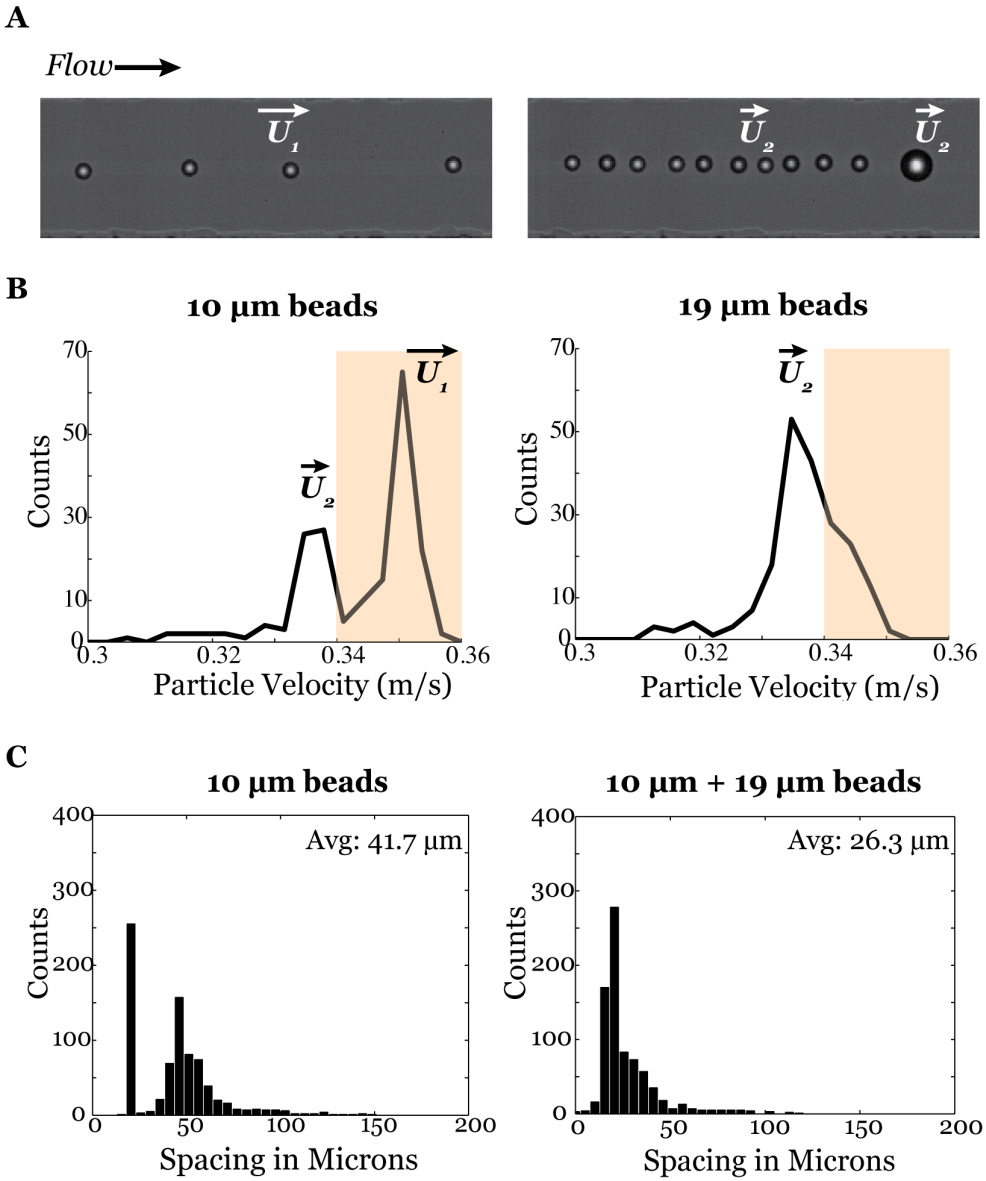

Fig. 3.1: Velocities and spacing of mixed particle populations. (A) *High-speed images of particle trains formed by small beads and mixed beads. Images are from the same experiment. Large beads lead particle trains of mixed populations.* ***(B)*** *10-µm beads exhibit two velocities. The faster velocity, U_1, does not exist for the 19-µm bead population. The two velocities are attributed to the two observed scenarios depicted in (A).* ***(C)*** *Spacing histograms show mixed populations of 10-µm and 19-µm beads have a lower average interparticle spacing (26.3 µm) than 10-µm beads alone (41.7 µm). Data was taken 47 mm downstream of inlet. Channel dimensions: H=30 µm and W=80 µm.*

The reason for the observed variation in velocities was not studied rigorously, but it is possible to make a few hypotheses. In a case of linear shear, different sized particles centered at the same location would be expected to average to the same velocity; however, in this confined flow, the shear gradient across a particle is not a simple linear function. Therefore, it may be argued that integrating the streamlines spanned by the 19-μm particles could result in a lower overall average velocity. Since these large particles also span more than half of the channel height, they capture streamlines past the maximum parabolic velocity at the channel center and may thus result in a reduced velocity. It is also a possibility that the 19-μm particles are so large that their behavior is unlike previously studied particle-induced flows because they are closely approaching the channel dimensions and may be interacting with fluid at the channel walls and experiencing higher drag. Furthermore, the local velocity profile may not be a typical parabolic profile, but rather changed by the particle locally due to its size. Evidence of unique secondary flows induced around the large particles occurred during instances where smaller beads were trapped between two large beads (Fig. 3.2A). A normal velocity profile would lead to particle focusing at the top and bottom positions as viewed through the channel cross-section (Fig. 3.2B), but it was observed that the 10-μm particles instead adopted a "diamond" motif and were locally stabilized outside the normal focusing positions. This may be explained through a possible mechanism of induced secondary flows outlined in Fig. 3.2B, as predicted by the work of Amini *et al.* for flows around a particle located in the center of the channel.[25]

Since cells are heterogeneous in size, the concept of inherent spacing contraction due to velocity differences becomes important in designing a system that performs relevant analysis or separation before any induced expanded spacing effects dissipate and the cells return to a contracted state.

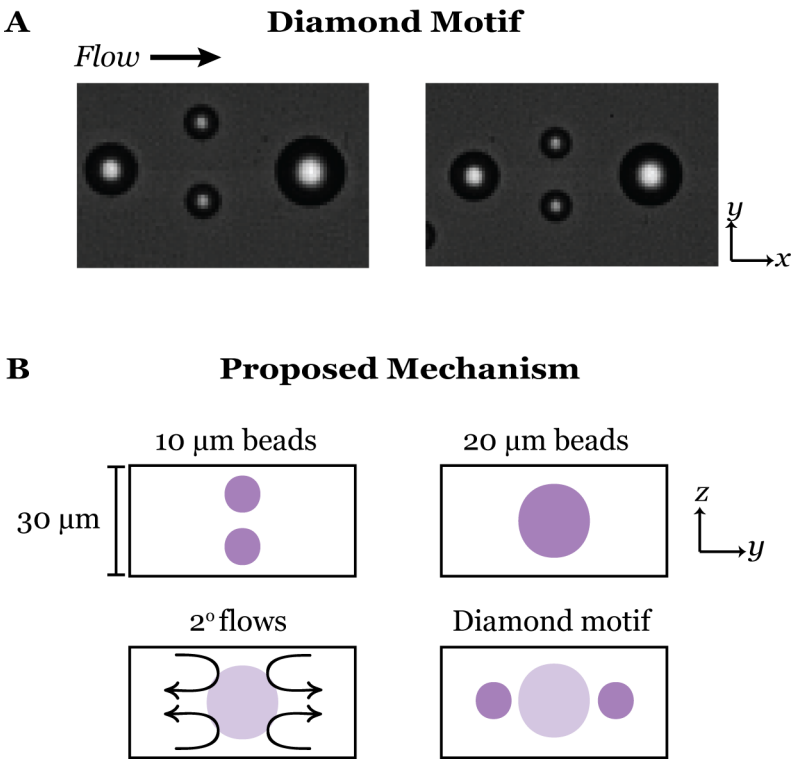

Fig. 3.2: Observed secondary flows caused by mixed particle populations and proposed mechanism. ***(A)*** *Small beads (10-μm) that were caught between large beads (19-μm) exhibited an unexpected focusing pattern. The small particles are in the same plane judging by the sizes of their shadows.* ***(B)*** *A proposed mechanism for this new focusing behavior is outlined. Drawings are to scale. Normally, 10-μm beads are expected to focus to top and bottom positions, as seen in the cross-section. A 20-μm bead approximately located at the center can be expected to induce secondary flows as shown, promoting the migration of particles at the top and bottom out towards the shorter walls of the cross-section. The small bead would be in the same plane and would have a "diamond" shape.*

3.2 Preliminary Designs

The aim of this work was to control interparticle spacing through changes to channel geometry alone. Initial designs of structured channels with localized expansion-contraction sections are summarized in Fig. 3.3. The channels were fabricated with a low aspect ratio (H = 30 μm, W = 80 μm), resulting in two particle-focusing positions at the center of the channels as viewed from the top (Fig. 3.4A). Particles were distinguished as being in same-stream or cross-stream configuration based on particle shadow differences caused by in- and out-of-plane focusing. A preliminary screening of these channels was conducted to select for

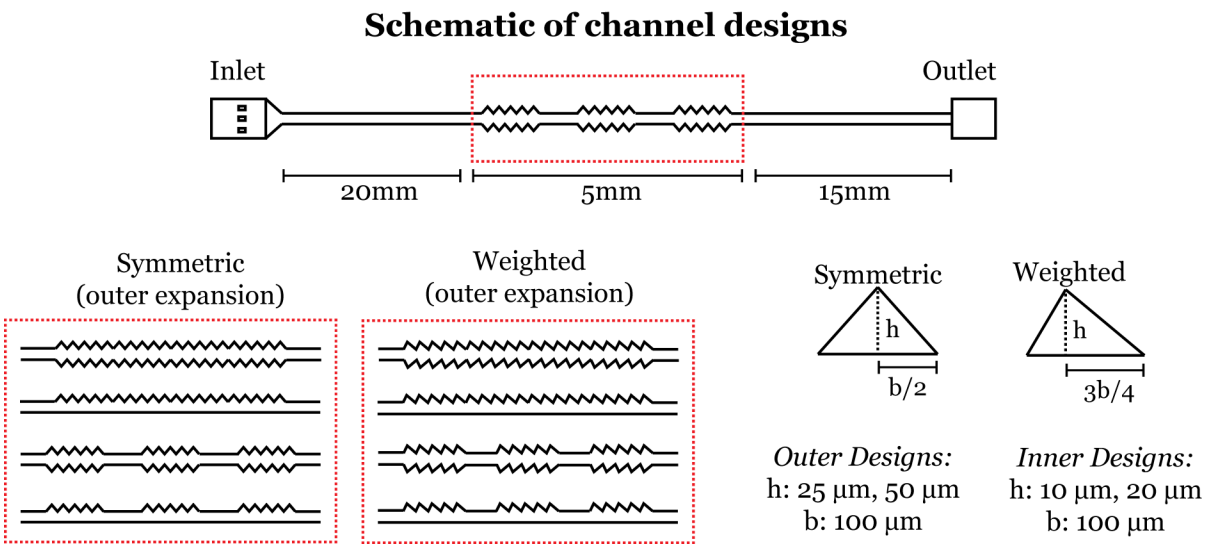

Fig. 3.3: Preliminary designs of structured channels. *A schematic of the microfluidic channel is provided (H = 30 μm, W = 80 μm). An initial 20mm straight channel section allows for inertial focusing of particles before entering the structured region. Structured regions spanned 5 mm, and consisted of various designs as summarized. For the cases of alternating structures, a total of 5 structures were used (only 3 are depicted here for simplicity). Dimensions of each individual symmetric and weighted expansion are displayed. Although only outer expansion designs are drawn here, dimensions for the inner designs that contracted from the original channel width are also provided for reference.*

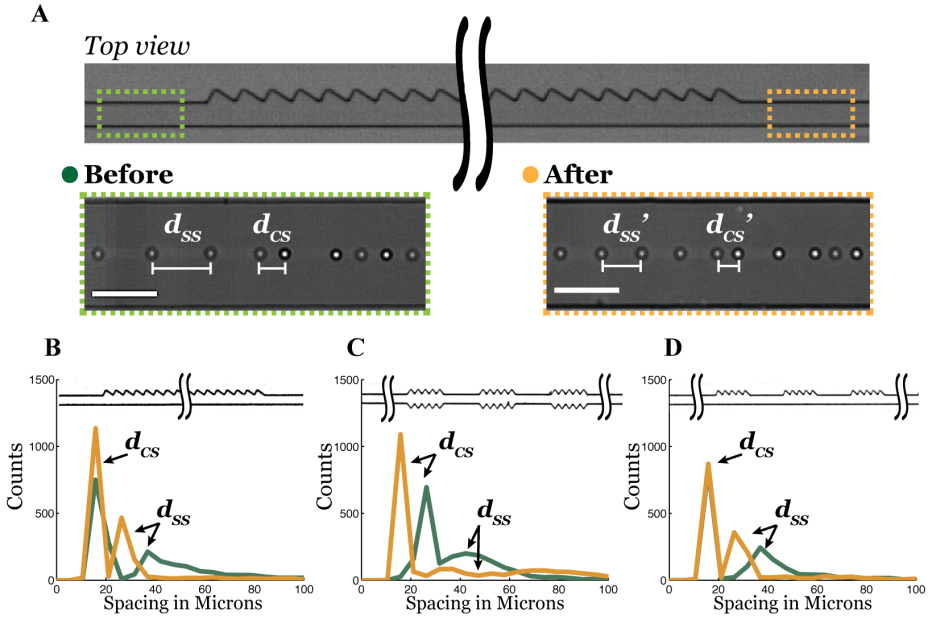

Fig. 3.4: Spacing effects of preliminary designs. ***(A)*** *High-speed images of particles before and after passing the structured section. A weighted design is shown in this example. Same-stream and cross-stream particles are distinguished by their in- and out-of-plane shadows, allowing their separation distance to be measured. Scale bar: 50 μm.* ***(B-D)*** *Histograms of interparticle spacing before and after structures. The "after" images are taken 12 mm downstream of structures. Weighted structures contract same-stream spacing (B, D) and symmetric structures (C) expand same-stream spacing. Cross-stream spacing is mainly unaffected.*

structured channels with the most favorable spacing effects. Fig. 3.4 provides an example of high-speed images obtained from these experiments, as well as histograms of interparticle spacing for select designs.

3.2.1 Spacing Effects

In general, structures that extended outward from the original channel width (outer designs) were more effective at producing spacing effects than structures that contracted inward and reduced the channel width (inner designs). Furthermore, it was noted that a minimum expansion width of 50 μm for this channel configuration (62.5% increase in channel width) was common to more effective designs. Weighted designs also tended to contract same-stream particle spacing, whereas symmetric designs were more suited towards expanding same-stream spacing. A summary of the interparticle spacing results for outer expansion designs is provided in Table 1.

Table 1: Summary of effects to interparticle spacing for outer expansion-contraction designs

		Symmetric	Weighted
50/100-μm Expansion	Full Section, Both Sides	**Δ**	**Δ**
	Full Section, One Side	**Δ**	**X**
	Alternating, Both Sides	**O**	**X**
	Alternating, One Side	**X**	**X**
25/100-μm Expansion	Full Section, Both Sides	**X**	**O**
	Full Section, One Side	**X**	**Δ**
	Alternating, Both Sides	**X**	**O**
	Alternating, One Side	**X**	**Δ**

X = No expansion, **Δ** = Some expansion, **O** = Strong expansion

With these results, a few channels were chosen for a more in-depth analysis. The 50/100 geometry of alternating, symmetric expansions on both sides of the channel had a strong

effect towards the expansion of interparticle spacing, and so was selected for further study. In contrast, it was noted that some structures with expansions only on one side of the channel, specifically the weighted structures, also caused contraction of spacing. To further understand this different behavior, weighted designs were also carried into the next-generation designs for more analysis. However, it is possible that several of the other designs with intermediate spacing effect may have also been valid candidates for integration into microfluidic channels for spacing control if they had been further optimized.

CONTROL OF INTERPARTICLE SPACING

4.1 Expansion of Spacing

The following describes how structured channels were used to achieve greater interparticle spacing and discusses system capabilities. It should be noted that particle spacing manipulation is possible due to the existence of voids between neighboring particle trains typical to microfluidic platforms, such that expanding spacing between particles results in the filling of these voids and creates more uniform spacing throughout the channel.

4.1.1 Local Expansion-Contraction Design

Symmetric expansion-contraction structures that alternated with sections of straight walls proved to have a strong effect in the expansion of same-stream interparticle spacing (refer to Fig. 3.4). To isolate this behavior, a high aspect ratio channel ($H > W$) with sheath fluid in co-flow with particle solution (Fig. 4.1) was designed with the same expansion-contraction structures to reduce the system to a single focusing position. Although in true application single-stream focusing might be achieved through inertial methods, this facilitates the analysis of same-stream particle interactions in structured channels.

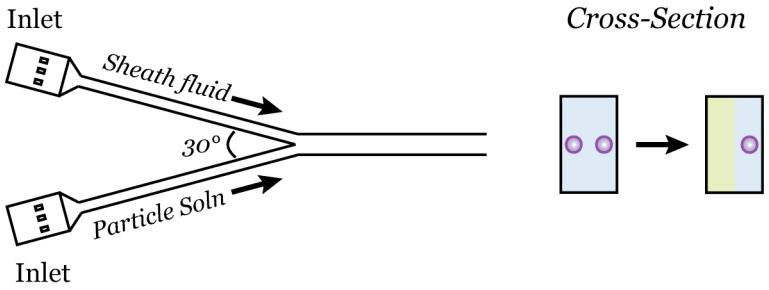

Fig. 4.1: Schematic for co-flow in high aspect ratio channel. *A sheath fluid is introduced with the particle solution to create single-stream focusing through the reduction of one equilibrium position.*

Spacing data before and after particles pass through the expansion-contraction structures shows the percentage of 10-μm beads (V_f = 0.5% solution) with interparticle spacing above 40 μm is consistently greater in structured channels than in straight channel controls (Fig. 4.2), similar to preliminary experiments. The structures were placed after a 2-cm section of straight channel to allow inertial focusing to take place. To understand the mechanism behind this observed expansion in spacing, fluid flow simulations using finite-element analysis were conducted to elucidate any patterns in the secondary flows caused by fluid passing through the structures in this channel configuration. Cross-sectional results show a secondary flow that pulls fluid from the top of the channel and circulates it outwards towards the vertical channel walls near the centerline (Fig. 4.3). This secondary flow would be expected to promote the movement of particles towards the walls when located at their equilibrium positions in the cross-section, as illustrated for a 10-μm particle. It should be noted that only the top half of the channel is depicted, but the results are symmetric across the x-axis.

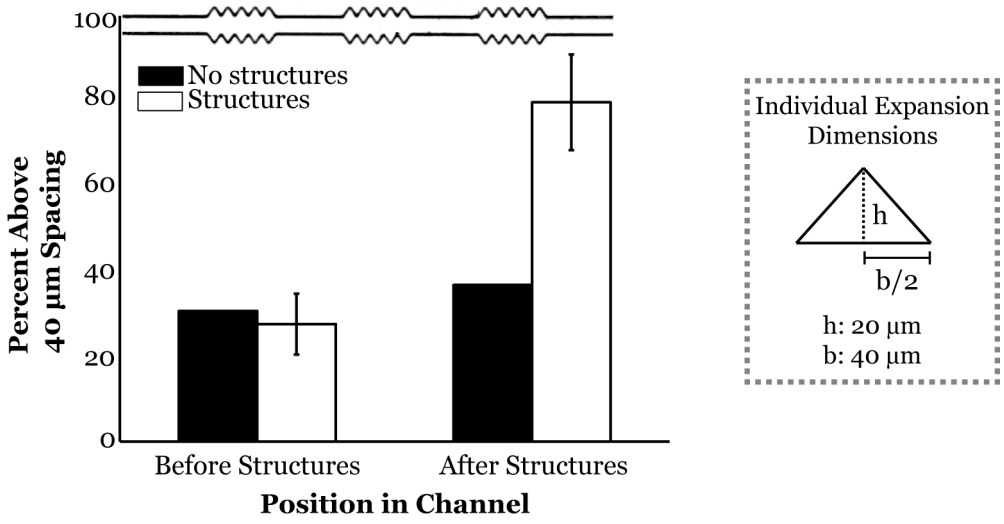

Fig. 4.2: Expansion of spacing in symmetric structured channels. *Structured channels increase the percentage of same-stream interparticle spacing above 40 μm compared to straight channel controls (Re = 12, V_f = 0.5%). Standard deviation calculated for experimental trials (n=5), each trial containing spacing data for approximately 2,000-4,000 beads. Images were taken 1 mm before and after the structures. Structures spanned 6 mm for a total of 12 sets of structures. Fabricated channel dimensions: H = 72 μm, W = 45 μm.*

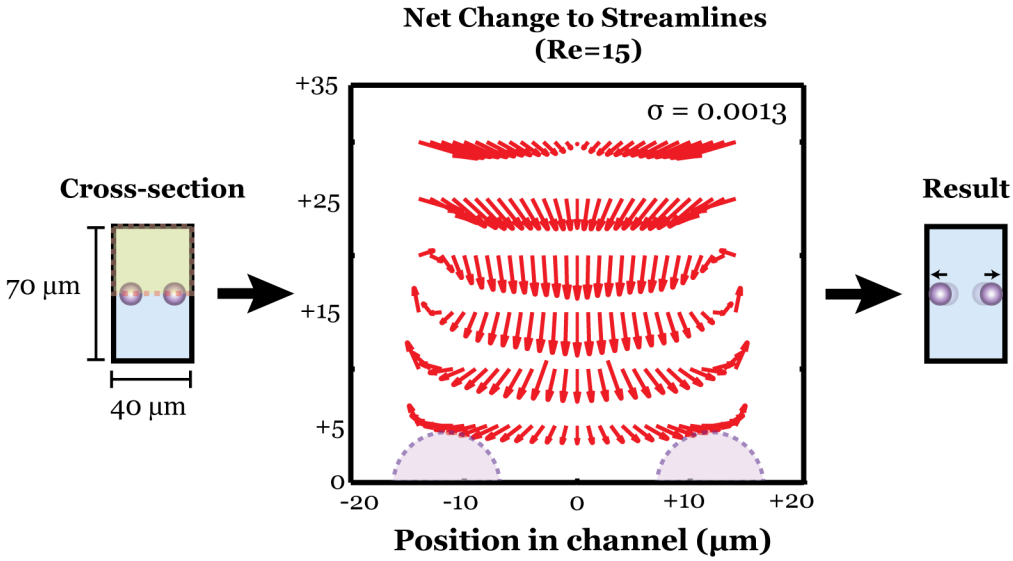

Fig. 4.3: Secondary flows caused by structures promote movement of particles towards channel wall. *Fluid flow in the top half of the channel was simulated using finite-element analysis. The net change to streamlines as they pass through 5 sets of structured sections is plotted for Re = 15. Fluid is pulled from the top of the channel and recirculated outwards towards the vertical channel walls at the channel centerline. 10-µm particles at equilibrium positions in this secondary flow would experience a net shift towards the channel walls, as depicted in the schematic. The strength (σ) of the flow field is equal to 0.0013 (nondimensional measure (max velocity/average velocity) from ref. 18).*

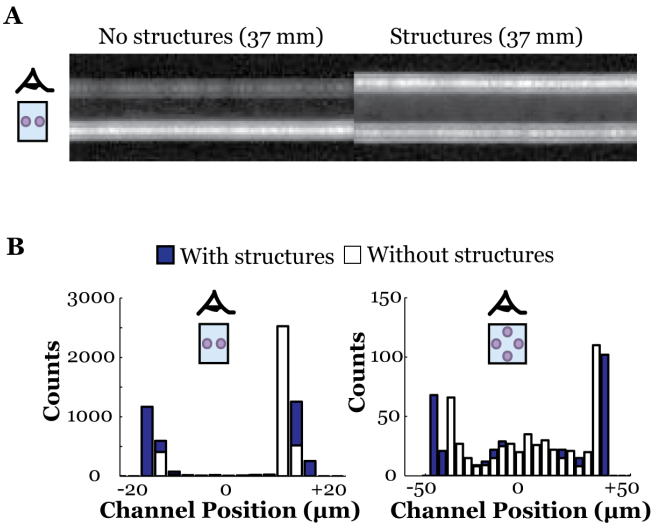

Fig. 4.4: Shift of equilibrium position in structured channels is confirmed experimentally. ***(A)*** *High aspect ratio channels with structures undergo a shift of particle focusing positions towards the walls in comparison to straight channel controls (2000 images overlaid for particle streaks).* ***(B)*** *Histograms of particle position for high aspect ratio and square channels support provide a quantitative measure of the shift (square channel data provided by Aram J. Chung).*

The shift of particles towards the walls was confirmed experimentally; particles passing through the structures were observed to laterally shift towards the channel wall in both square and high aspect ratio channels (Fig. 4.4). Since the controls do not demonstrate expansion to spacing, this difference in particle position in the channel became the basis for understanding the mechanism behind the ability of structured channels to cause changes to particle interactions and consequently, increase spacing.

Numerical simulations from the reference frame of the particle of fluid flow around particles positioned at their equilibrium position show the presence of repulsive recirculations (Fig. 4.5A) that have been reported as a mechanism leading to particle spacing[23,24]. The highest velocity of the recirculations was 0.157 m/s for an inlet fluid velocity of 0.3 m/s (Re=15). However, when the particle position was shifted closer to

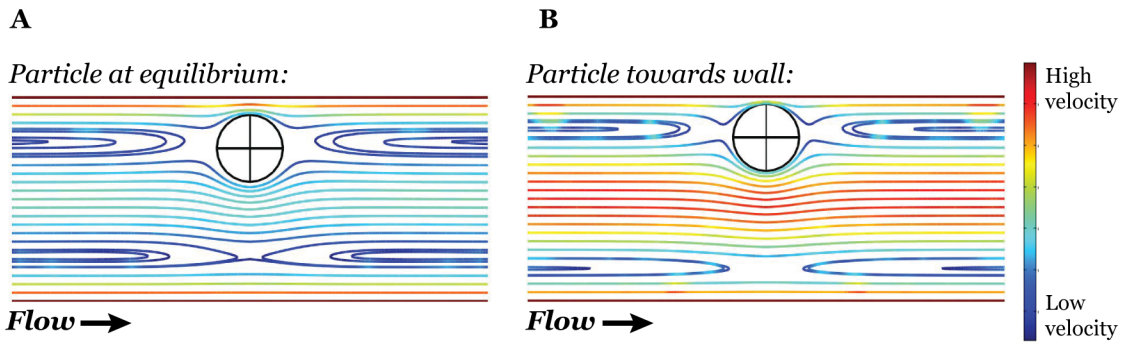

C

	At equilibrium	*Near wall*
Input fluid velocity	*0.3 m/s*	*0.3 m/s*
Strength of recirculation	*0.16 m/s*	*0.23 m/s*

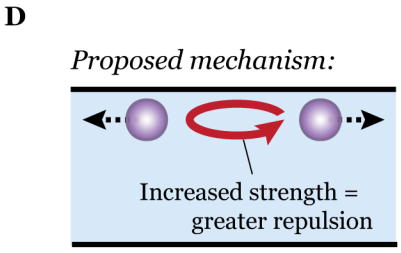

Fig. 4.5: Repulsive interactions strengthened between particles with focusing position closer to channel wall. ***(A)*** *Fluid flow simulations of a particle at its normal equilibrium position depict entrained recirculations responsible for normal particle spacing (Re = 15).* ***(B)*** *A particle that has shifted its position closer to the channel wall has recirculations with increased strength, as tabulated in* ***(C)****.* ***(D)*** *The proposed mechanism for particle spacing expansion brought on by shift of the equilibrium position: an increased strength in the recirculations leads to greater repulsion between particles*

the wall (Fig. 4.5B), the recirculations caused by the particle had a higher velocity of 0.230 m/s. Recirculation velocity values were found by locating the outermost streamline of the recirculation and measuring the velocity. The streamlines towards the center of the recirculation approach zero, and so the outermost streamline can be expected to have the largest effect on the particles.

This increase in velocity suggests that the recirculations are strengthened, and are more capable of creating stronger repulsive interactions between particles (Fig. 4.5D). It is then proposed that the mechanism for expansion of interparticle spacing in structured channels is a result of the secondary flows the structures induce, which promote a shift of particles towards the channel walls and lead to the strengthening of the viscous disturbance flows that make up recirculations surrounding the particles. This in turn results in a stronger repulsion between particles and results in an expansion in interparticle spacing.

4.1.1.1 Effect of Flow Rate

The expansion of spacing through the use of local expansion-contraction structures was conserved across various flow rates. Using co-flow for single-stream focusing, the results indicate similar efficacy of the structures as *Re* increases (Fig. 4.6). The average interparticle spacing and the percent above 40 μm for 10-μm particles increase slightly with higher values of *Re*, except for the highest value of *Re* = 30. In this case, it appears that there is no significant effect of the structures to expanding spacing. To begin with, the amount of particles entering the structures at *Re* = 30 with spacing greater than 40 μm was notably greater than for the other test cases, indicating that the initial conditions during the experiment were not alike.

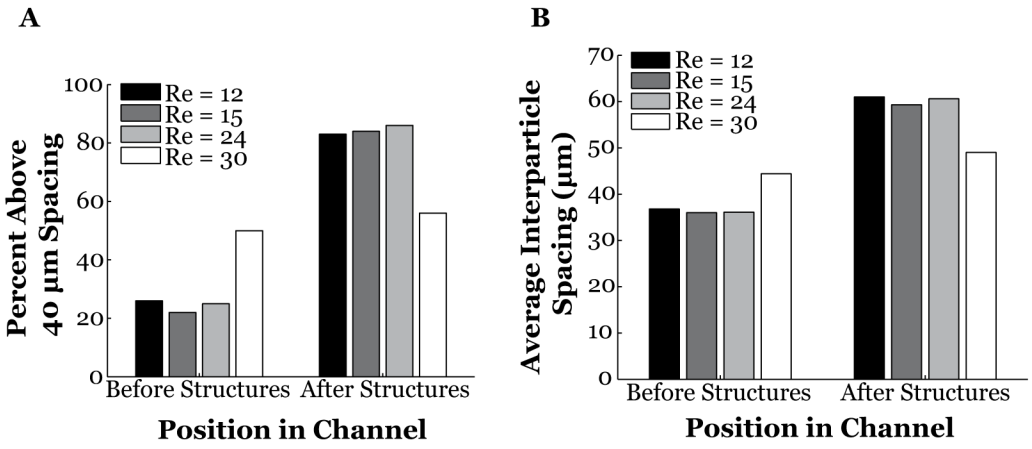

Fig. 4.6: Expansion of interparticle spacing is conserved for various Reynolds numbers. ***(A)*** *The percent of particles above 40-µm spacing is increased after passing through symmetric local expansion-contraction structures, except for the case of Re = 30.* ***(B)*** *The average interparticle spacing in microns is shown for various flow rates. Channel dimensions: H = 72 µm, W = 45 µm. (a = 10 µm, V_f = 0.75%)*

Nonetheless, it can still be expected that the structures should enhance the population of particles above 40-µm spacing if the direction of the secondary flow predicted for *Re* = 15 in the numerical simulation is conserved across varying *Re*. However, with the above results, it is possible that the secondary flows adopt a different orientation as *Re* is varied. Numerical simulation across different values of *Re* for structured channels may elicit further understanding of this observation, and may offer a working range for the expansion of particle spacing.

4.1.1.2 Effect of Concentration

The ability of these structured channels to operate over a range of concentrations is important in supporting high-throughput platforms. The expansion of spacing, however, is highly dependent on the presence of voids (regions lacking particles) in order for particle trains of tight spacing to be expanded into the gaps provided by voids. At extremely high concentrations, the amount of voids present between long chains of particle trains is reduced, thereby limiting particle manipulation and expansion. It was previously discussed how a length fraction (λ) of 0.25 (one 10-µm

particle per 40-μm section of fluid) is the maximum value for an ideal solution of uniformly spaced particles in order to ensure a minimum spacing of 40 μm (refer to Section 3.1.1). In reality, length fractions and volume fractions are representative of the average spacing, meaning that there will be particle pairs below the desired minimum spacing in any given suspension. As the length fraction increases over 0.25, the challenge to expanding 100% of particles to a minimum of 40 μm grows.

Structured channels were tested at various concentrations to observe their efficiency at expanding interparticle spacing. At λ = 0.4, structured channels enhanced the population of particles above 40-μm spacing to 83%; however, at a value of λ = 0.2, this effect was increased to 98% (Fig. 4.7).

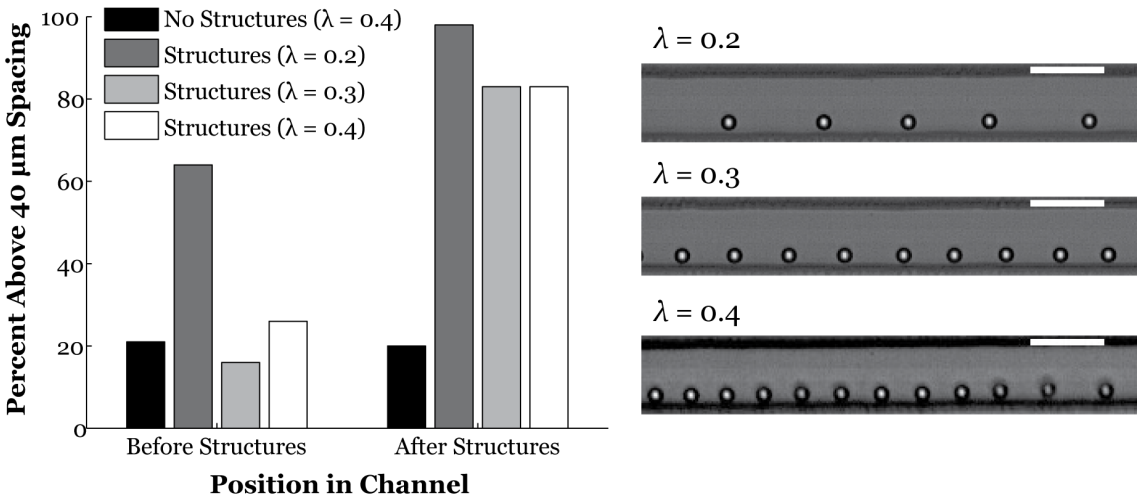

Fig. 4.7: Effect of concentration to particle spacing expansion. *Particle suspensions of lower concentration and lower length fraction (λ =0.2) are more effectively expanded by symmetric local expansion-contraction structures. As the concentration increases, this efficiency drops. This difference is due to the reduction of voids between particle trains at high concentrations.*

4.1.2 Chamber Design

The local expansion-contraction designs proved to have favorable expansions of same-stream interparticle spacing, particularly for concentrations where voids are present between particle trains. To compare it to previous work that has been suggested to also affect interparticle spacing, an extended expansion-contraction structure similar to the work of Lee *et al.*[23] was designed and tested. The extended expansion-contraction section, or chamber, was placed after a 2-cm straight channel region to allow particles to inertially focus prior to entering the chamber. The changes to interparticle spacing as 10-μm particles entered a chamber of width 2.3x the original channel width are presented for various flow rates (Fig. 4.8). The chamber length spans 1 mm, channel dimensions are H = 72 μm and W = 45 μm, and V_f =0.5%. In this scenario, Re = 30 was not formally recorded due to the large amount of particle collisions and defocusing that occurred in the chamber.

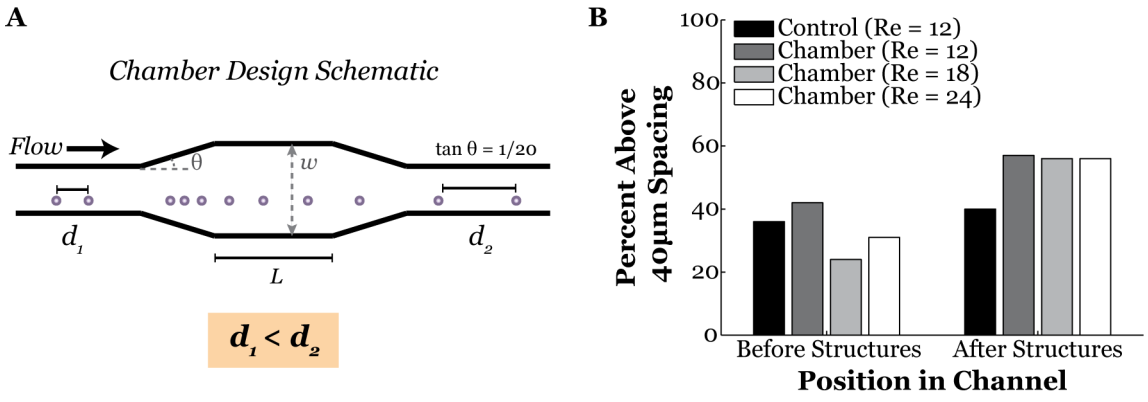

Fig. 4.8: Expansion of spacing with chamber design. *(**A**) Schematic of design and particle behavior. The interparticle distance is greater upon exiting the chamber. The length of the expansion (L) was 1 mm, the width of the expansion (w) was 70 μm. The original channel width W = 40 μm.* ***(B)*** *The percent of particles above 40 μm is slightly enhanced for channels containing a chamber. However, the percentages are lower than for local expansion-contraction designs (>80%).*

These results indicate that the amount of expansion possible from the use of extended chambers is less than that observed with local expansion-contraction structures. However, they do provide some expansion in comparison to control channels, and may be useful if further optimized (different chamber width, length of chamber).

The mechanism for this method of particle expansion has been previously described[23]. Briefly, as fluid enters and fills the expansion region, the particles are slowed due to conservation of mass. This momentarily brings the particles closer together, and consequently results in viscous repulsive forces that push the particles apart within the chamber. As they exit the chamber region, the particles are further spaced as fluid returns and reach a distance greater than their entry distance[23].

4.1.3 Combined Design

The local expansion-contraction structures were able to locally affect interparticle spacing and lead to its expansion; however this capability was limited at higher concentrations when large particle trains were formed and voids were infrequent because the structures were limited to a more local effect and could not cause massive reorganization. In other words, particle pairs and small trains that are traveling through the structures are more easily fine-tuned and repelled to greater distances than long, continuous particle trains that require more bulk movement of numerous particles.

The chamber design was not as effective at expanding spacing reliably, but did exhibit more global particle control. Particles beyond 100 μm of spacing could be brought together as they entered the chamber and would reorganize to a more uniform particle train as they exited (Supp. Fig. A and B). This bulk rearrangement provides a potential

tool to achieve more global particle control that is absent in local expansion-contraction structures.

Given these observations, it was hypothesized that a combination of both types of structures could result in improved expansion of spacing due to their different acting mechanisms for particle control. The results indicate that the expansion of spacing is indeed enhanced when the local structures and chamber are placed in series relative to the performance of either one of the structures alone (Fig. 4.9). High aspect ratio channels were fabricated to test for single-stream focusing similar to previous experiments.

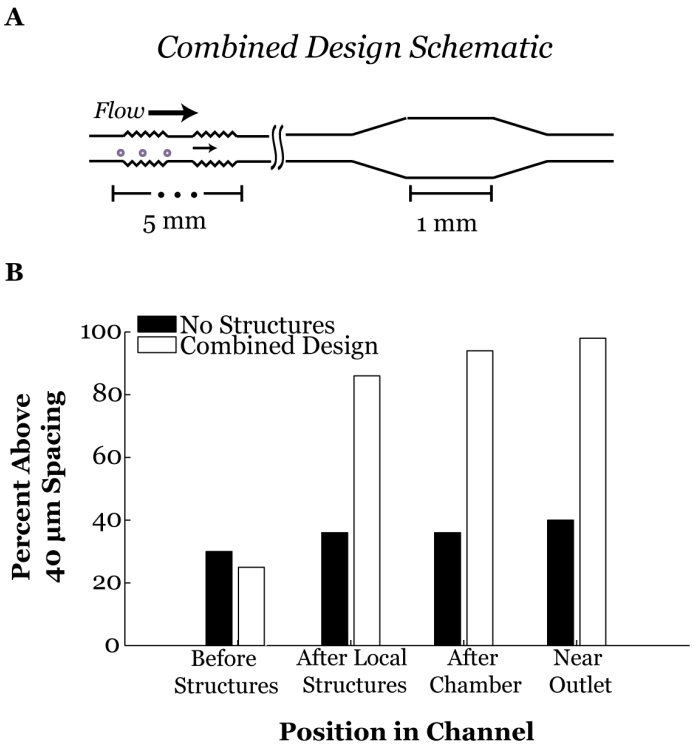

Fig. 4.9: Local structures and extended chamber in series improve expansion of spacing at high concentrations. *The combination of both structures causes an increase to the percent of particles above 40 µm near the outlet (98%) when compared to each structure alone. This was achieved at lower flow rate (Re = 12) and high particle length fraction (λ = 0.4). Expansion is 2.3x original channel width. Particle diameter is 10 µm.*

The chamber was tested in locations before and after the local structures, and the results showed no difference to the effectiveness of spacing. A variety of chamber dimensions were tested to optimize for particle control. In the case of too large or too sudden of an

expansion, particles were likely to collide and defocus due to the weakening of the wall effect lift force that stabilizes particles to their equilibrium positions (Fig. 4.10). This was undesired, since particles need to be in focused trains to maintain the particle interactions necessary for control. Results also show that larger expansions provide better expansion of spacing (Fig. 4.11).

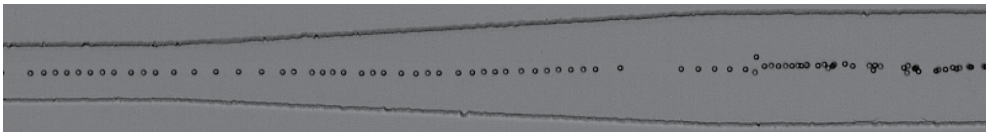

Fig. 4.10: Particle defocusing in sudden chamber expansion. *High-speed images show particle collisions and defocusing when chamber width is too large or expansion is too sudden. Defocusing occurs due to the disappearing wall effect lift force that maintains particles focused to their equilibrium positions as the channel width expands.*

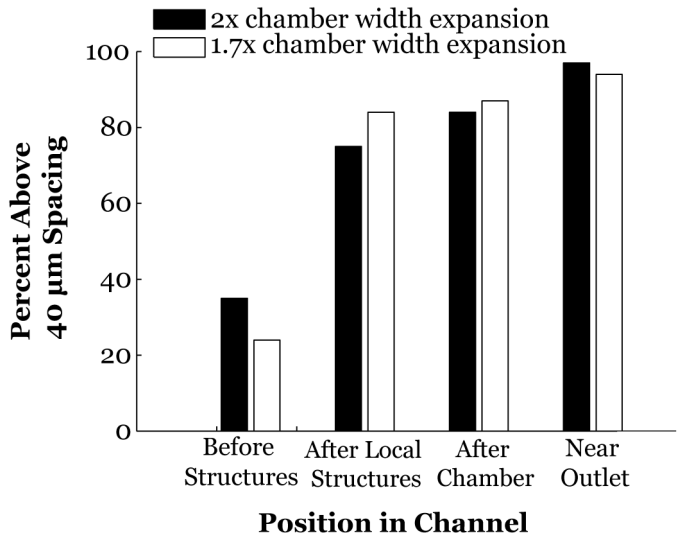

Fig. 4.11: Larger chamber width promotes more expansion of spacing. *Near the outlet, the percent of particles above the desired threshold is greater in the case of the larger chamber expansion (98% vs. 94%). In these specific experiments, a = 10 μm, V_f = 0.5% and Re = 12. The original channel width before expansion is 30 μm. The channel height is 60 μm.*

4.2 Contraction of Spacing

An unexpected finding was the sensitivity of particle spacing to the shape of the structures such that a weighted expansion on one side of the channel could lead to contraction of spacing. The results and proposed mechanism are outlined below.

4.2.1 Weighted Design

Preliminary results indicated that interparticle spacing was contracted with specific weighted and asymmetric designs (refer to Table 1). This was further investigated using a high aspect ratio channel (H = 72 μm, W = 45 μm) and co-flow of sheath fluid and particle solution (a = 10 μm, V_f = 0.5%). Interestingly, when single-stream focusing was studied, it was noted that the interparticle spacing was expanded, not contracted, immediately after the structures, and was marginally more expanded than the controls further downstream (Fig. 4.12). However, when no sheath fluid was used and two

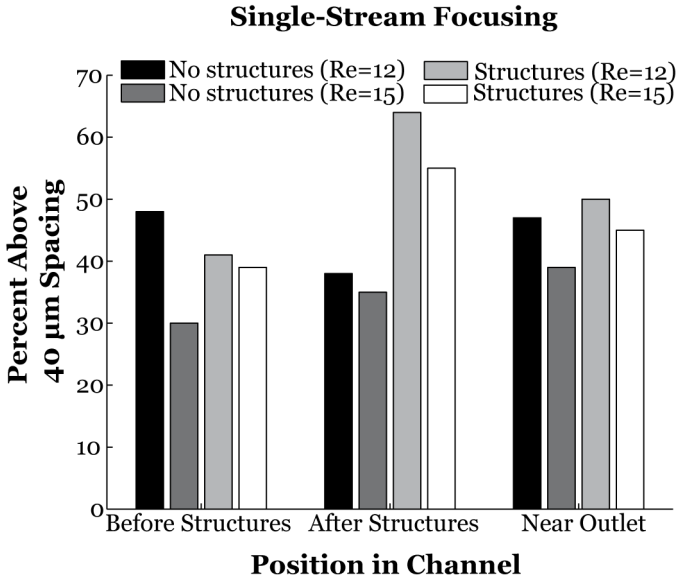

Fig. 4.12: Single-stream focusing in weighted structures results in marginal expansion of spacing. *Weighted structures cause an increase to the expansion of spacing immediately after the structures when compared to straight channel controls, but this effect dissipates downstream. The structured channels are comparable to controls near the outlet.*

particle streams were present, the spacing was expanded immediately after the structures but was again noted to slightly contract downstream, as in preliminary experiments (Fig. 4.13).

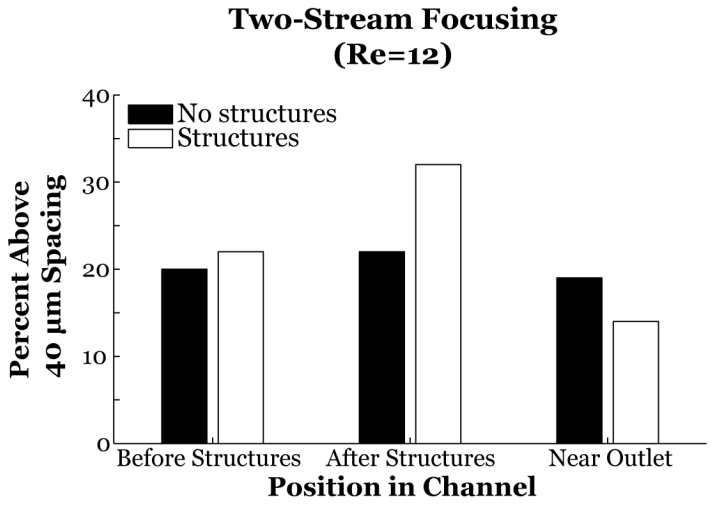

Fig. 4.13: Two-stream focusing in weighted structures results in contraction of spacing. *Weighted structures cause an increase to the expansion of spacing immediately after the structures when compared to straight channel controls, but this effect is reversed downstream. The structured channels have a reduced population of expanded particles compared to inlet conditions and compared to the control.*

To understand this behavior, fluid flow simulations for weighted structures were prepared and analyzed for the induced net change to streamlines across the structures. The resulting normalized vector plot of the channel cross-section shows asymmetric secondary flows (Fig. 4.14). Under single-stream focusing, particles were introduced into the right-half portion of the channel (as depicted), and so experienced only the weaker secondary flow patterns that do not promote a strong displacement from the equilibrium position, as was the case in the symmetric structures (refer to Fig. 4.3). Conversely, with two-stream focusing, particles on the left half of the channel can be expected to undergo a net movement towards the channel wall.

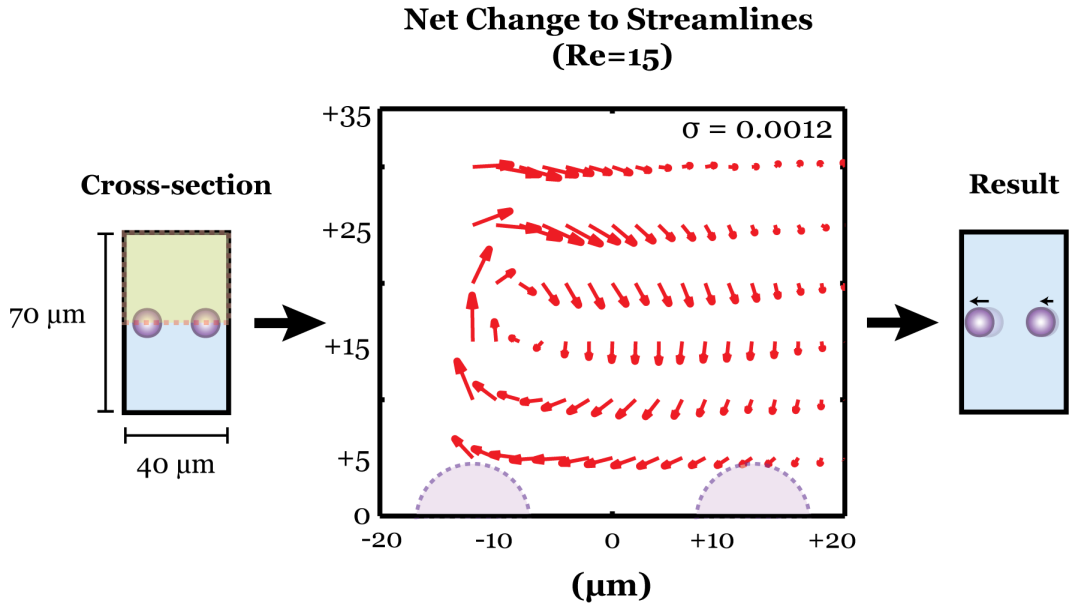

Fig. 4.14: Weighted, asymmetric structures cause asymmetric secondary flows. *Fluid flow in the top half of the channel was simulated using finite-element analysis. The net change to streamlines as they pass through 5 sets of weighted sections is plotted for Re = 15. Fluid is pulled from the top left corner of the channel and recirculated clockwise. The asymmetric strength in the secondary flow will cause 10-µm particles focused in the left position (as depicted) to experience a net lateral movement towards to wall), while particles on the right experience a weaker push towards the channel centerline. The strength (σ) of the flow field is equal to 0.0012 (nondimensional measure (max velocity/average velocity) from ref. 18).*

Considering the parabolic velocity profile in confined flows, particles closer to the wall are expected to travel slower than those closer to the channel centerline. This results in two particle streams traveling at different speeds. It is then suggested that in the case of weighted or asymmetric structures, contraction of spacing occurs when particles are present in both focusing positions because particles traveling in the faster stream will approach those in the slower stream and experience cross-stream interactions that lead to compression of the particle train. This also supports the results of experiments with single-stream focusing, since there were no cross-stream interactions to cause contraction of spacing. Furthermore, it is likely that the slight expansion of spacing in single-stream weighted designs was similar to the controls near the outlet because the

particle stream was not brought closer to the wall and the repulsive interactions in the reversing streamlines were not strengthened (as was the mechanism of expansion in symmetric structures). The temporary expansion of spacing immediately after the structures is possibly a result of particles being momentarily brought closer together in the expansion sections as a matter of conservation of mass; however, this effect does not last far downstream, potentially because the particle interactions are not altered more permanently, such as through a shift in equilibrium position. In preliminary experiments, images were not obtained immediately after the structures but were instead collected after 12 mm. It is likely that even in these preliminary experiments, a similar amount of expansion may have occurred immediately following the weighted structures but was not recorded.

4.3 Spacing Effects of Mixed Populations

Heterogeneous populations are common to most relevant biological samples, and so it is important for a system that controls interparticle spacing to be able to function under mixed populations. Previously listed experiments were conducted with 10-μm particles of CV (coefficient of variation) less than 5%. Typical cancer cell populations (such as MCF-7 breast cancer cells or Jurkat leukemia cells) have an average diameter of ~12-14 μm and a CV of ~15-20%. In this next section, cells and larger beads with a higher CV were tested with the combined structure design outlined in Section 4.1.3.

4.3.1 Heterogeneous Beads

Preliminary experiments demonstrated how larger particles traveled at a lower velocity than smaller particles and led to the contraction of interparticle spacing in straight channels. A bead population of 15-μm particles with CV = 14%, was introduced into the combined structure design to observe if the effects could be reversed.

15-μm beads in straight channel controls exhibited a contraction to interparticle spacing, as expected (Fig. 4.15A). However, in the case of structured channels, the effect was slightly reversed (Fig. 4.15B). Taking a closer look after each structure, the results indicate that the local expansion-contraction structures were able to increase the interparticle spacing immediately following the structures, but this full effect did not last far downstream. As particles reached the outlet, the spacing effects were mostly lost and the percent of particles above 40 μm was almost returned to the initial conditions.

The use of structured channel can thus be used to overcome the contraction of interparticle spacing that occurs in heterogeneous populations. The expansion effects are particularly more prominent immediately following the local structures, before the natural contraction returns, and so placement of particle analysis components in close proximity to the structures is an important design consideration.

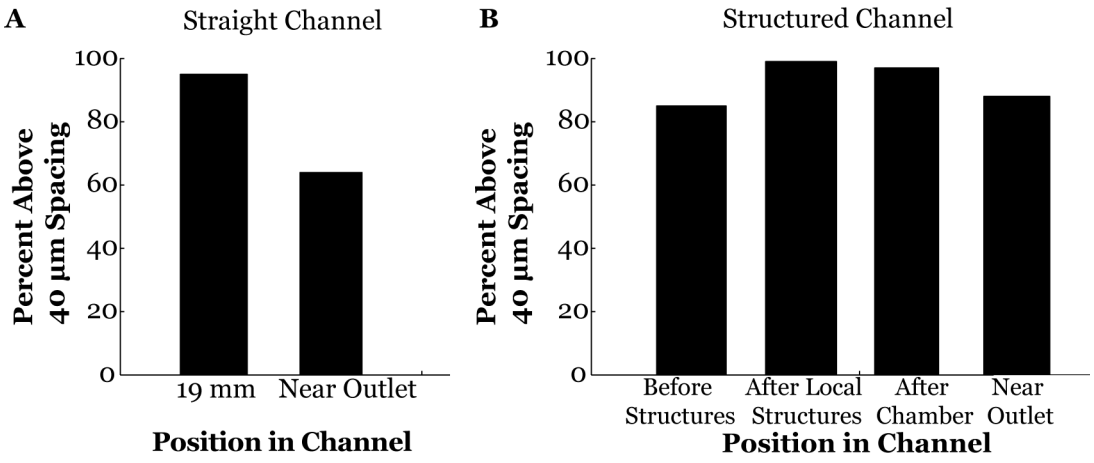

Fig. 4.15: Inherent contraction of spacing for mixed bead populations is reversed using structured channels. ***(A)*** *In straight channel controls, interparticle spacing of 15-μm beads (CV = 14%) is contracted as particles travel down the channel. Images were taken at 19 mm (same location as in all previous experiments) and near outlet (47 mm).* ***(B)*** *Structured channels with both local structures and extended chamber reverse this observed contraction. The percent of particles above the threshold increases to 99% after local structures compared to inlet conditions (85%). This effect, however, slightly dissipates as particles continue to travel down the channel and reach the outlet (88%).*

4.3.2 Cells

Following the characterization of the structured channels with beads of low and high CV, the system was tested for its spacing capability with cells. Jurkat cells (avg. diameter = 12 μm, CV = 16%) at a concentration of 3.4 million cells/mL were introduced into a high aspect ratio channel and the same-stream interactions were studied.

High-speed images of the channel illustrate how the cells behave similar to the 15-μm bead population tested previously. The expansion effects caused by structured channels are strong immediately following the structures, but also dissipate near the outlet (Fig. 4.16A). A quantitative measure of the spacing shows that the spacing is expanded compared to control channels with no structures (Fig. 4.16B).

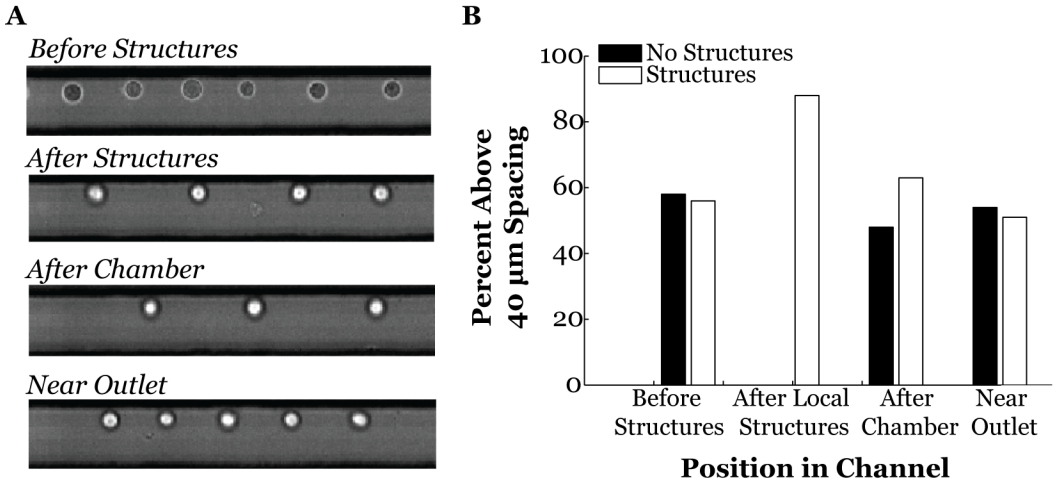

Fig. 4.16: Inherent contraction of spacing for cells is reversed using structured channels. ***(A)*** *High-speed images illustrate the changes to cell spacing before and after structures. It can be seen how the reduced spacing returns once cells reach the outlet (47mm).* ***(B)*** *Structured channels with both local structures and extended chamber reverse this observed contraction of cell spacing. The percent of cells above the threshold increases to 88% after local structures compared to inlet conditions (56%). This effect, however, dissipates as cells travel down the channel and reach the outlet (51%). Channel dimensions: H = 72 μm, W = 45 μm. Cell suspension concentration used for these experiments was 3.4 million cells/mL. (No data was recorded for the control in an equivalent location to "after local structures.")*

This behavior of expanded spacing in cells and mixed bead populations after the structures agrees with previous experimental results with monodisperse bead populations. The secondary flows induced by the structures likely have a similar effect on cells and mixed bead populations, resulting in a strengthened repulsion between neighboring particles. The effects, however, do not carry far downstream as in the case of same-sized beads. This is possibly because the shift of particles towards the walls is not permanent, and as cells and mixed particles relax to their equilibrium positions, the spacing is again contracted by their inherent differences in velocities.

CONCLUSION

This work is the first exploration into passive particle and cell spacing control using structured channels in an inertial microfluidics platform, and at its current stages can provide improvement to interparticle spacing for systems that operate at high throughputs. The use of local expansion-contraction structures to induce secondary flows that promote lateral migration of particles towards the wall, thereby strengthening interparticle repulsions and increasing spacing, has shown to be effective with changing Reynolds numbers, high and low concentrations, and heterogeneous populations of beads and cells. Furthermore, implementing extended expansions for bulk particle manipulation has shown to often improve the expansion of particle spacing when placed after local structures, making this system for particle control more robust for implementation into single-cell analysis applications.

REFERENCES

1. Nagrath, S. *et al.* Isolation of rare circulating tumour cells in cancer patients by microchip technology. *Nature* **450**, 1235–9 (2007).

2. Wu, T.-H. *et al.* Pulsed laser triggered high speed microfluidic fluorescence activated cell sorter. *Lab Chip* - (2012).doi:10.1039/C2LC21084C

3. Hur, S. C., Mach, A. J. & Di Carlo, D. High-throughput size-based rare cell enrichment using microscale vortices. *Biomicrofluidics* **5**, 22206 (2011).

4. Mach, A. J., Kim, J. H., Arshi, A., Hur, S. C. & Di Carlo, D. Automated cellular sample preparation using a Centrifuge-on-a-Chip. *Lab on a chip* **11**, 2827–34 (2011).

5. Gossett, D. R. *et al.* Label-free cell separation and sorting in microfluidic systems. *Analytical and bioanalytical chemistry* **397**, 3249–67 (2010).

6. Gossett, D. R. *et al.* Inertial Manipulation and Transfer of Microparticles Across Laminar Fluid Streams. *Small (Weinheim an der Bergstrasse, Germany)* 1–8 (2012).doi:10.1002/smll.201200588

7. Goda, K. *et al.* High-throughput single-microparticle imaging flow analyzer. *Proceedings of the National Academy of Sciences of the United States of America* 1–6 (2012).doi:10.1073/pnas.1204718109

8. Oakey, J. *et al.* Particle focusing in staged inertial microfluidic devices for flow cytometry. *Analytical chemistry* **82**, 3862–7 (2010).

9. Hur, S. C., Henderson-MacLennan, N. K., McCabe, E. R. B. & Di Carlo, D. Deformability-based cell classification and enrichment using inertial microfluidics. *Lab on a chip* **11**, 912–20 (2011).

10. Gossett, D. R. *et al.* Hydrodynamic stretching of single cells for large population mechanical phenotyping. *Proceedings of the National Academy of Sciences of the United States of America* **109**, 7630–5 (2012).

11. Guck, J. *et al.* Optical deformability as an inherent cell marker for testing malignant transformation and metastatic competence. *Biophysical journal* **88**, 3689–98 (2005).

12. Hur, S. C., Tse, H. T. K. & Di Carlo, D. Sheathless inertial cell ordering for extreme throughput flow cytometry. *Lab on a chip* **10**, 274–80 (2010).

13. Di Carlo, D. & Lee, L. Dynamic single-cell analysis for quantitative biology. *Analytical chemistry* **78**, 7918–25. (2006).

14. Edd, J., Carlo, D. D. & Humphry, K. Controlled encapsulation of single-cells into monodisperse picolitre drops. *Lab Chip* **8**, 1262–1264 (2008).

15. Kemna, E. W. M. *et al.* High-yield cell ordering and deterministic cell-in-droplet encapsulation using Dean flow in a curved microchannel. *Lab on a chip* (2012).doi:10.1039/c2lc00013j

16. Heikali, D. & Di Carlo, D. A Niche for Microfluidics in Portable Hematology Analyzers. *Journal of the Association for Laboratory Automation* **15**, 319–328 (2010).

17. Fuh, C. B. Split-flow Thin Fractionation. *Analytical chemistry* **72**, 266–271 (2000).

18. Di Carlo, D. Inertial microfluidics. *Lab on a chip* **9**, 3038–46 (2009).

19. Segré, G. & Silberberg, A. Behaviour of macroscopic rigid spheres in Poiseuille flow Part 1. Determination of local concentration by statistical analysis of particle passages through crossed light beams. *Journal of Fluid Mechanics* **14**, 115 (1962).

20. Di Carlo, D., Irimia, D., Tompkins, R. G. & Toner, M. Continuous inertial focusing, ordering, and separation of particles in microchannels. *Proceedings of the National Academy of Sciences of the United States of America* **104**, 18892–7 (2007).

21. Carlo, D. D., Edd, J. F., Humphry, K. J., Stone, H. A. & Toner, M. Particle Segregation and Dynamics in Confined Flows. *Engineering in Medicine* **094503**, 1–4 (2009).

22. Gossett, D. R. & Di Carlo, D. Particle focusing mechanisms in curving confined flows. *Analytical chemistry* **81**, 8459–65 (2009).

23. Lee, W., Amini, H., Stone, H. a & Di Carlo, D. Dynamic self-assembly and control of microfluidic particle crystals. *Proceedings of the National Academy of Sciences of the United States of America* **107**, 22413–8 (2010).

24. Matas, J.-P., Glezer, V., Guazzelli, E. & Morris, J. F. Trains of particles in finite-Reynolds-number pipe flow. *Physics of Fluids* **16**, 4192 (2004).

25. Amini, H., Sollier, E., Weaver, W. M. & Di Carlo, D. Intrinsic particle-induced lateral transport in microchannels. *Proceedings of the National Academy of Sciences of the United States of America* 1–6 (2012).doi:10.1073/pnas.1207550109